TU Delft
Challenging Glass 2 – Conference on Architectural and Structural Applications of Glass, Bos, Louter, Veer (Eds.), TU Delft, May 2010.

Modeling the Structural Response of Reinforced Glass Beams using an SLA Scheme

Christian Louter
Faculty of Architecture, TU Delft, The Netherlands / ICOM, EPFL, Switzerland
p.c.louter@tudelft.nl
Anne van de Graaf, Jan Rots
Faculty of Civil Engineering & Geosciences, TU Delft, The Netherlands
a.v.vandegraaf@tudelft.nl, j.g.rots@tudelft.nl

This paper investigates whether a novel computational sequentially linear analysis (SLA) technique, which is especially developed for modeling brittle material response, is applicable for modeling the structural response of metal reinforced glass beams. To do so, computational SLA results are compared with experimental results of four-point bending tests. The results show similarities in load-displacement curves and to some extent also in cracking behaviour. Overall, it is concluded that the SLA scheme is a very promising technique to model the structural response of reinforced glass beams, which will be even further improved in future research.

Keywords: computational analysis, reinforced glass, brittle, saw-tooth.

1. Introduction

The main challenge of modeling the structural response of reinforced glass beams is the extremely brittle behaviour of glass. Due to this brittle response, non-linear numerical analyses often run into convergence problems. To address the problem of brittle material response, a sequentially linear elastic analysis (SLA) technique is currently under development at Delft University of Technology.

The main concept of this SLA technique, which was introduced by Rots [1] and further developed by Rots, Belletti and Invernizzi [2, 3], De Jong et al. [4] and Van de Graaf et al. [5], is to replace the 'standard' incremental-iterative analysis scheme by a series of scaled linear analyses, while at the same time the nonlinear stress-strain law is replaced by a saw-tooth reduction curve. In this way, a possibly negative tangent stiffness, which is the main cause of convergence problems in non-linear analyses, is avoided.

Preliminary investigations of Van de Graaf [6], using the SLA technique to model the structural response of reinforced glass beams, showed promising results. From that study it was concluded that the SLA technique seems to give more realistic results – particularly regarding the snapback behaviour which is automatically included – than standard non-linear numerical analyses. However, a comparison with experimental results has not been made in that study.

The current study therefore investigates the validity of the SLA technique for modeling the structural response of reinforced glass beams by comparing the results of SLA analyses to experimental results of four-point bending tests performed on 1.5 m reinforced glass beams [7]. Additionally, the consistency of the SLA approach has been investigated by varying several model parameters.

The following sections describe the experimental and computational setup. Furthermore, the results of the experiments and analyses are described, compared and discussed. Finally, conclusions from the study are provided.

2. Experimental and Computational Setup

2.1. Beam model

Figure 1 shows the cross-sections of both the physical beam specimens and the computational 2D beam model. The physical beams consist of three layers of annealed float glass, which have been bonded together with a stainless steel (grade 304L) reinforcement section using a UV-curing acrylate adhesive. For the computational model this beam geometry has been simplified to a full glass section with an equivalent thickness and a reinforcement truss with an equivalent cross sectional area.

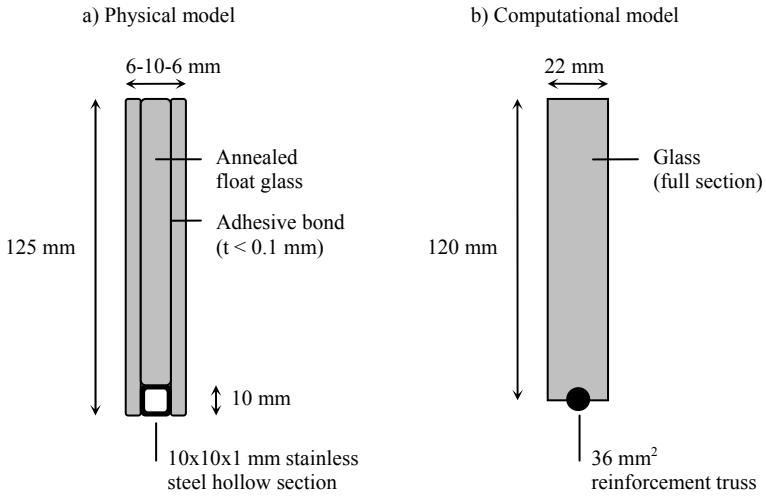

Figure 1: Cross sections of a) the physical beams and b) the computational model.

2.2. Experimental and computational procedure

The physical beam specimens have been tested in four-point bending using a conventional testing machine, which has been provided with a specially designed support frame, see Figure 2a. The beams have been loaded at a displacement rate of 2 mm/min until initial glass failure occurred. Subsequently, the load was removed to investigate the crack pattern. Thereafter, the beams have been reloaded at a vertical displacement rate of 5 mm/min until complete failure. During the tests the applied load and the vertical displacement of the cross-head, see Figure 2a, have been measured.

For the computational 2D model the same load and support spans have been used as for the experimental test setup, see Figure 2b. In the computational model the glass of the beam has been discretized using quadratic plane stress elements, while the reinforcement has been built up from quadratic truss elements. The following steps have been performed during the computational procedure [5]:

a) Perform a linear-elastic analysis with a representative (unit) load.
b) Determine which element has the largest maximum stress over tensile strength ratio (i.e. identify the critical element).
c) Scale the representative load such that a critical stress state is obtained.
d) Update the stiffness and strength properties of the critical element in accordance with a user defined reduction scheme (saw-tooth curve).
e) Repeat steps a to d continuously until the damage has spread into the beam sufficiently.

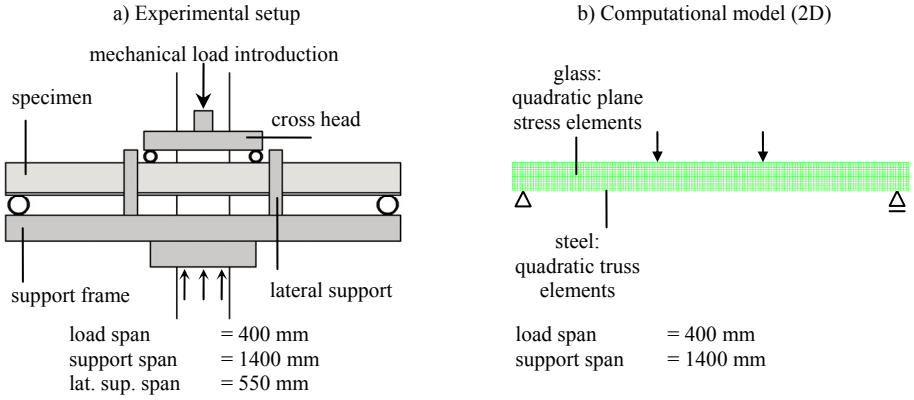

Figure 2: a) Experimental setup, and b) Computational model.

2.3. Material parameters

The physical beams have been composed of annealed float glass, stainless steel reinforcement and a polymer adhesive bond. For the computational model the glass and reinforcement have been modeled as homogeneous isotropic materials with initial materials parameters as provided in Table 1. However, for the glass, upon crack initiation at some point, the initially isotropic constitutive matrix of that point is being replaced by an orthotropic matrix. Additionally, reduction curves have been defined for both the glass and the reinforcement, which will be discussed in the following subsections. The adhesive bond between the individual glass sheets and between the glass and reinforcement has not been incorporated in the computational model, see Figure 1. For current study a perfect bond between the glass and reinforcement has been assumed and no adhesive parameters have been defined.

Table 1: Adopted material parameters for glass and stainless steel roughly based on [8, 9, 10].

			Annealed glass	Stainless steel
Young's modulus	E	MPa	70 x10^6	190 x10^6
Poisson's ratio	ν	-	0.23	0.265
Tensile strength (initial)	f_t	N/mm^2	45	550
Fracture energy	G_f	J/m^2	3	-

For the glass a 'saw-tooth' reduction curve has been defined following the construction technique proposed by Trovato [11], see Figure 3a. During the computational analysis the stiffness and strength of a critical glass element will be reduced following this curve which will simulate cracking of that specific element. The saw-tooth curve has been constructed based on a mother curve, see Figure 3a, which represents the 'standard' stress-strain law for glass and shows a snapback at constitutive level. The area underneath the mother-curve equals the fracture energy of glass G_f divided by a certain crack band width h. For square quadratic elements the crack band width has been assumed equal to the length of an element side. The saw-tooth reduction curve has been constructed in such a way that the fracture energy associated with the saw-tooth curve matches the fracture energy associated with the mother curve.

For the stainless steel reinforcement a similar reduction curve has been implemented in the computational model to simulate yielding of the reinforcement section. This reduction curve has been constructed based on a uniaxial tensile test on the metal reinforcement, see Figure 3b.

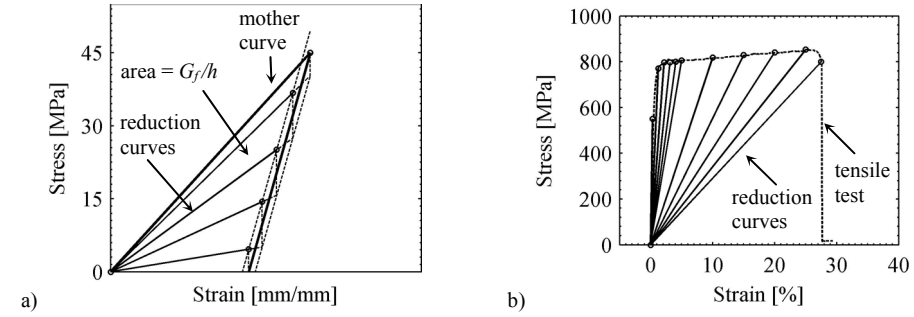

Figure 3: Exemplary reduction curves for a) glass, with 5 reduction steps, and b) steel with 10 reduction steps.

2.4. Variation of model parameters

To simultaneously investigate the dependency of the SLA technique to various model parameters, a series of computational models has been made within which these parameters have been differed, see Table 2. Firstly, the number of reduction steps for both the glass and reinforcement has been differed between 5 and 10, see models A-D. Secondly, the shear retention factor β has been varied between 0.001, 0.01, 0.1 and 1 respectively, see models C, E-G. This shear retention factor defines the reduction in shear stiffness for a 'cracked' element. The value of the factor should meet $0 \leq \beta \leq 1.0$, in which 0 represents no shear retention thus full reduction in shear stiffness, whereas 1.0 represents full shear retention thus no reduction in shear stiffness. Finally, the size of the elements has been differed between 5 and 10 mm square, see models C and H.

Table 2: Overview of the computational models with varying reduction steps and shear retention factors.

			A	B	C	D	E	F	G	H
Reduction steps glass	rs_{gl}	[-]	**5**	**10**	**5**	**10**	5	5	5	5
Reduction steps steel	rs_{st}	[-]	**5**	**5**	**10**	**10**	10	10	10	10
Shear retention factor	β	[-]	0.01	0.01	**0.01**	0.01	**0.001**	**0.1**	**1**	0.01
Mesh size	h	[mm]	10	10	**10**	10	10	10	10	**5**

3. Results

3.1. Experiment

The results of the 5 bending tests are presented in Figure 4, which shows the load-displacement curves (a) and a sequential set of diagrams indicating the crack development (b). The beam specimens showed linear elastic response until upon initial failure a V-shaped crack in the glass occurred, which originated from the tensile zone. This crack generally ran through all glass layers of the beam and travelled on average 86% of the beam height leaving the compression zone uncracked. Additionally, some adhesive failure and debonding of reinforcement has been observed upon initial failure along several centimetres on either side of the crack origin. During the reloading process in the second test run one or two additional V-shaped cracks occurred. The reinforcement started to progressively debond and the cracks in the glass started to propagate horizontally. For four beams final failure occurred due to full debonding of reinforcement. The tensile forces could not be transferred anymore and the beams collapsed. The other beam did not fail within the deformation capacity of the test setup.

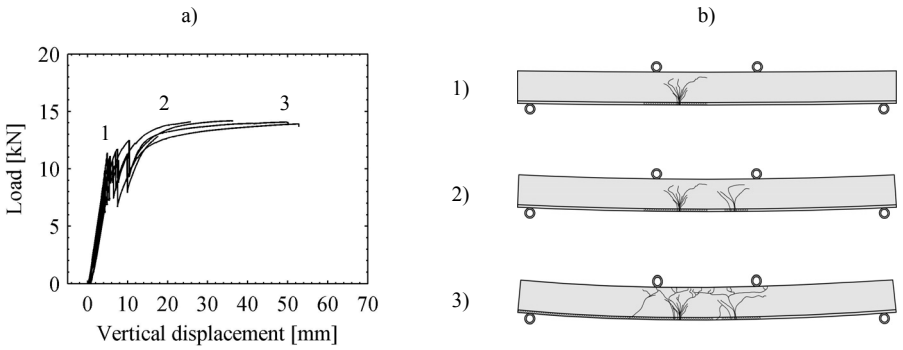

Figure 4: a) Load-displacement diagrams and b) cracking sequence of the experiments.

3.2. Computational model

As an example the results of the computational model A are shown in Figure 5. The results of the other models will be provided and discussed in Section 4. The load-displacement diagram presented in Figure 5a consists of a point cloud, which typically results from the sequence of linear elastic calculations, and a highlighted upper curve. For the ease of reading and interpreting, only the highlighted upper curve will be provided upon discussing the other model results. Additionally, Figure 5b shows a sequence of contour plots of the reduced E-modulus at both the glass and reinforcement elements. These plots have been generated at a vertical displacement level of 2, 5, 10, 20, 30, 40 and 50 mm and indicate the crack development in the beam.

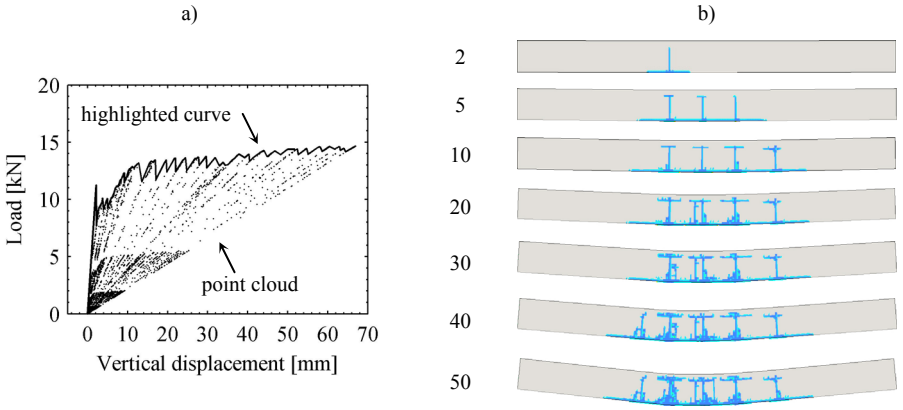

Figure 5: a) Load-displacement diagram and b) contour plots of the reduced E-modulus (crack pattern) resulting from the computational model.

4. Discussion

4.1. Comparison of computational and experimental results

Overall, the results of the computational analyses are in fairly good agreement with the experimental results. As can be seen in Figure 6, even the most basic model A, with a limited number of reduction steps for both the glass and steel (rs_{gl} = 5, rs_{st} = 5), gives a load-displacement diagram which is largely in agreement with the experimental results. The computational model reaches a similar post-breakage strength level and shows a similar reduction in beam stiffness at the post-breakage stage due to increased cracking of the glass and yielding of the reinforcement. Furthermore, as can be seen from Figures 4b and 5b, also the crack development within the computational model is, at least to some extent, similar to the experimental results. Similar to the experimental results, the computational model shows initial vertical crack growth followed by horizontal crack propagation. However, also some differences between the computational and experimental results can be observed.

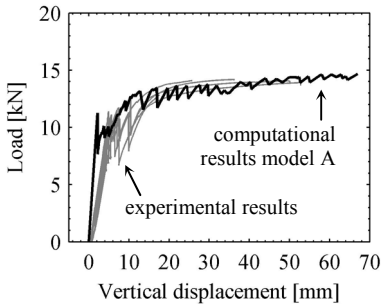

Figure 6: Combined load-displacement diagrams of the computational model A and the experimental results.

Firstly, the initial beam stiffness at the linear elastic stage differs between the computational and the experimental results. This difference is explained by the deflection of the steel support frame that has been used during the experiments. As can be seen in Figure 2a, the steel frame is only supported at mid-span and will deflect once a load is inflicted on the glass beam specimen. Since the vertical deformation within the test setup has been measured at the cross-head, see Figure 2a, the experimental results include both the deflection of the glass beam and the steel support frame, whereas the deflection of the steel support frame has not been included in the computational model.

Secondly, the computational models show mainly straight and vertically orientated cracks in the glass, whereas the experiments show V-shaped cracks, see Figures 4b and 5b. This difference is largely explained by the regular and square mesh geometry. It is expected that the application of an irregular and triangular mesh might alter the crack path and might lead to V-shaped cracks in the computational model. Additionally, the application of a rotating crack model, instead of the currently applied fixed crack model, might even further improve the shape of the cracks in the computational model. However, the SLA technique is not yet suited for the application of a rotating crack model. This will be further implemented in future developments of the SLA approach.

Thirdly, the computational model overestimates the amount of cracks in the glass. The experimental results only show two or three large cracks in the glass, but the computational model shows at least 4 or 5 cracks. This difference is probably the result of the absence of an adhesive bond in the computational model. Whereas the experiments show local adhesive failure and consequent debonding of reinforcement along several centimeters on either side of a crack origin in the glass, the computational model assumes a perfect bond between glass and reinforcement without the possibility of debonding. As the reinforcement debonded during the experiments, the forces could not be transferred anymore along this path, which caused a significant stress reduction at the edge of the glass and frustrated any new cracks to occur along this path. For the computational model this process was not incorporated and more extensive cracking occurred than for the experiments.

Finally, whereas the beams during the experiments finally failed due to full debonding of reinforcement, this failure mechanism did not occur for the computational model. Obviously, this difference is caused by the perfect bond between glass and reinforcement which has been assumed in the computational model. To allow the beams to fail due to debonding of reinforcement, the model should incorporate an interface between the glass and reinforcement which allows for bond-slip. These interface elements are not yet available in the SLA approach, but are currently under development.

4.2. Effect of number of reduction steps

Increasing the number of reduction steps for the glass does not alter the computational results. Although the number in reduction steps for the glass has been increased for model B (rs_{gl} = 10, rs_{st} = 5) compared to model A (rs_{gl} = 5, rs_{st} = 5), they yield perfectly similar results, see Figures 7a and 7b. The same is valid for models C (rs_{gl} = 5, rs_{st} = 10) and D (rs_{gl} = 10, rs_{st} = 10), see Figures 7a and 7c. From this observation it is concluded that the material behaviour of the glass can be rather accurately captured in the computational model using only a relatively limited number of reduction steps.

Increasing the number of reduction steps for the steel reinforcement does alter the computational results. Whereas the load-displacement curves of models A and B (both with rs_{st} = 5) show frequent load drops at the post-breakage stage, the load-displacement curves of models C and D (both with rs_{st} = 10) show a smoother trajectory at the post-breakage stage, see Figure 7a. Due to the increased number of reduction steps, the yielding of the steel reinforcement is more accurately followed in the computational model. This leads to smoother post-breakage curves which are more in line with the experimental results. However, it should be noted that increasing the number of reduction steps for the steel reinforcement also leads to a small increase in post-breakage strength level, see Figure 7a. Future research will investigate whether a further increase in reduction steps for the steel will lead to a further increase and possible overestimation of the post-breakage strength. Finally, it is observed that increasing the number of reduction steps for the steel does not significantly alter the cracking behaviour, see Figures 7b and 7c.

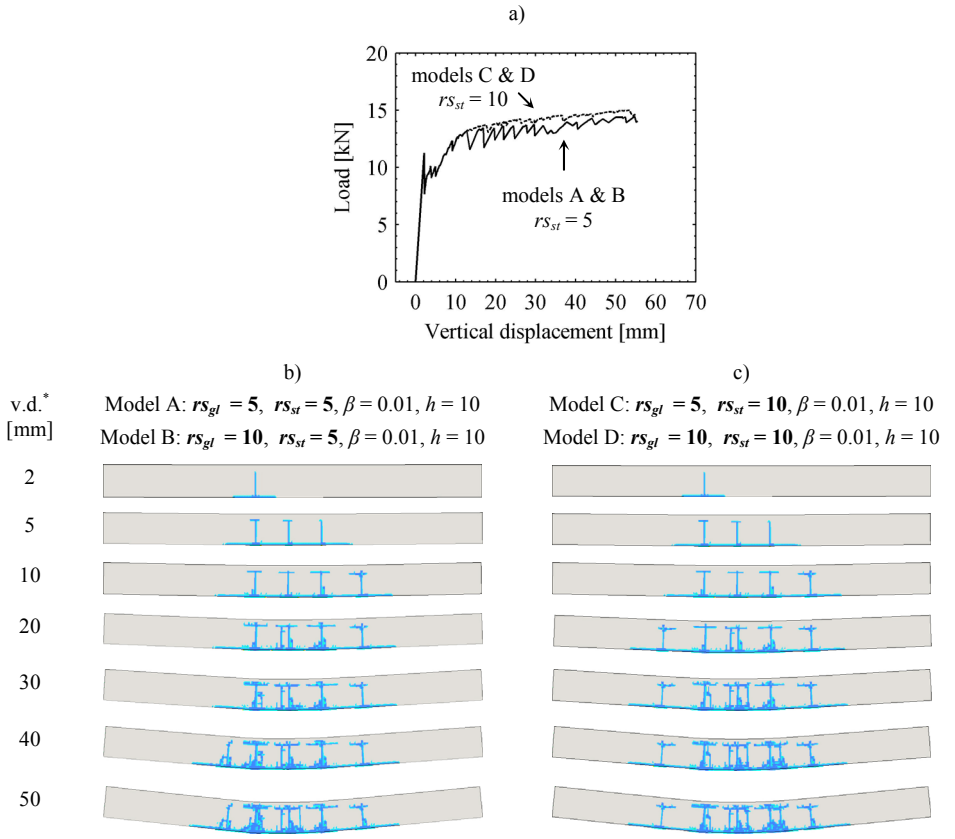

Figure 7: a) Load-displacement diagrams of models A, B, C and D with varying reduction steps;
b) contour plot of the reduced E-moduli (crack pattern) of model A and B;
c) contour plot of the reduced E-moduli (crack pattern) of model C and D;
*v.d. = vertical displacement

4.3. Effect of shear retention factor β

Varying the shear retention factor leads to only a small variation in the load-displacement curves, see Figure 8a. However, it does significantly affect the cracking behaviour of the beam models, see Figures 8b and 8c. Whereas model E with a very low value of β = 0.001 shows a relatively limited number of cracks, model G with the highest possible value of β = 1 shows highly extensive cracking. Due to the high shear retention factor the amount of shear force transferred by the 'cracked' elements is not reduced. This causes more extensive stressing of the neighboring/surrounding elements, which in turn start to crack. However, this more extensive cracking is not in line with the experimental results. A relatively low shear retention factor of β = 0.01 yields a cracking sequence which is largely in agreement with the experimental results.

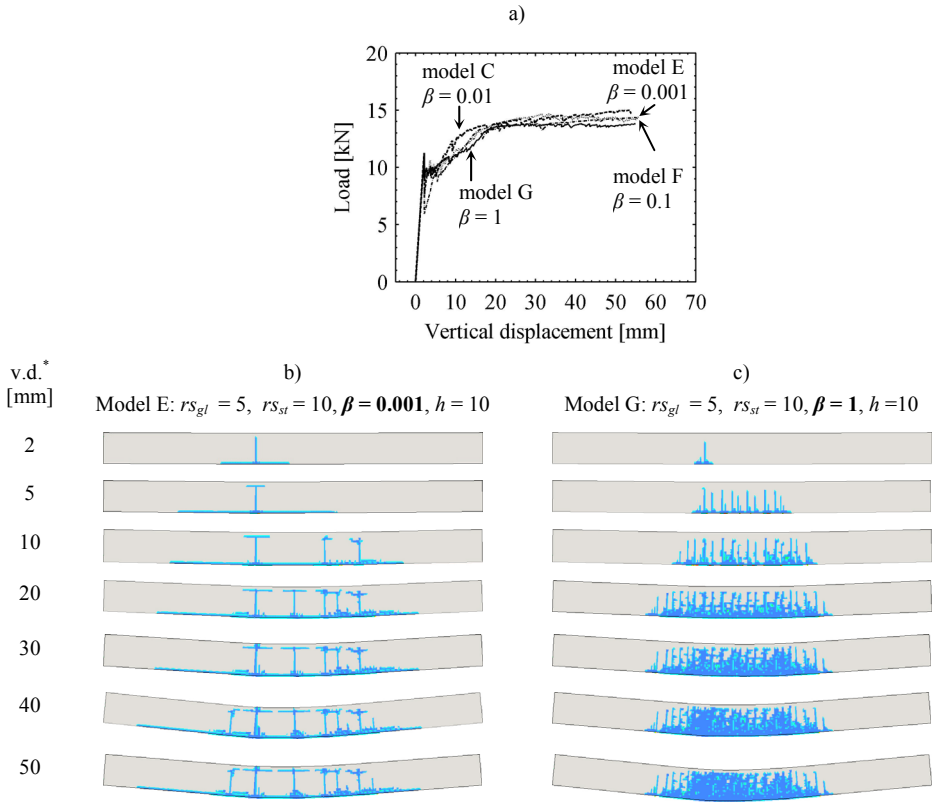

Figure 8: a) Load-displacement diagrams of models C, E, F and G with varying shear retention factors;
b) contour plot of the reduced E-moduli (crack pattern) of model E;
c) contour plot of the reduced E-moduli (crack pattern) of model G;
*v.d. = vertical displacement

4.4. Effect of mesh size

Mesh refinement, as has been done for model H (h = 5 mm) compared to model C (h = 10 mm), results in only small differences in the load-displacement curve, see Figure 9a. However, the cracking behaviour changes when the mesh is refined. As can be seen from Figures 9b and 9c, model H (with h = 5 mm) shows significantly more vertical cracks than model C (with h = 10 mm). Furthermore, model H shows a tendency for diagonal shear cracks, whereas this is not observed for model C. A similar effect of increased cracking and diagonal shear cracks due to mesh refinement has been observed by Van de Graaf [6]. However, a specific explanation for this effect has not been found yet and needs further investigation.

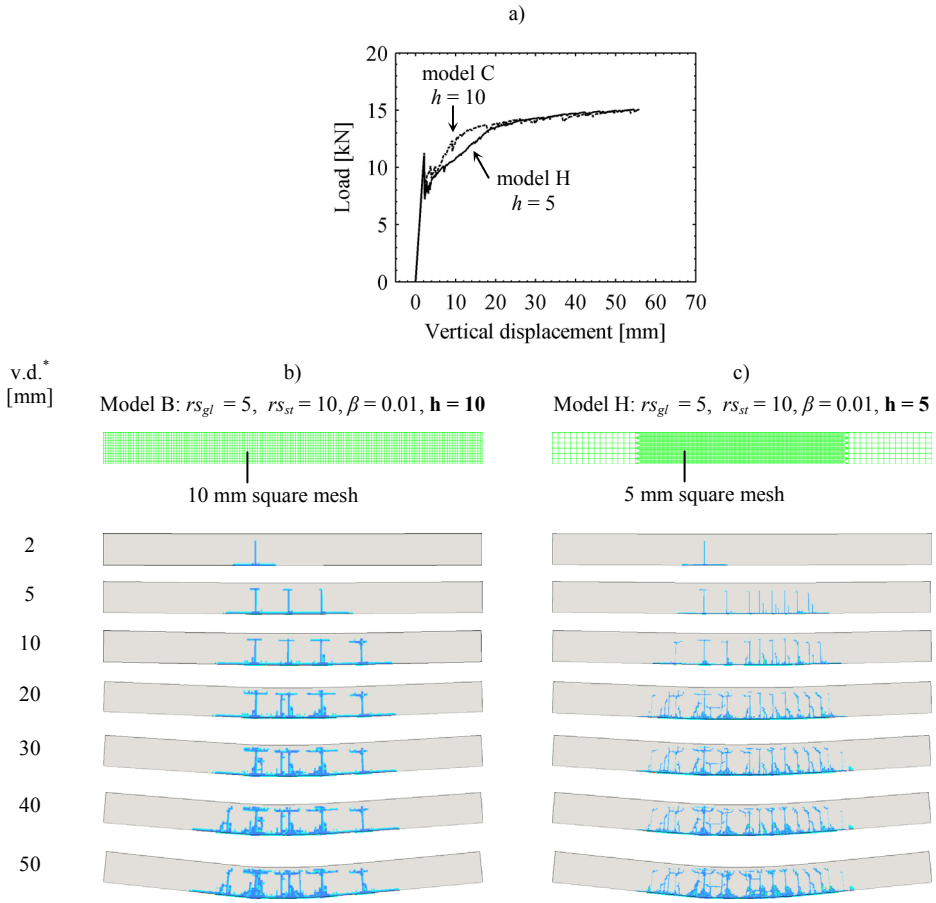

Figure 9: a) Load-displacement diagrams of models C and H with varying mesh sizes;
b) contour plot of the reduced E-moduli (crack pattern) of model C;
c) contour plot of the reduced E-moduli (crack pattern) of model H;
*v.d. = vertical displacement

5. Conclusions

From the comparison of the computational SLA results with the experimental results, it is concluded that the SLA approach offers a promising technique for modeling the structural response of metal reinforced glass beams. Especially in terms of load-displacement curves the computational model yields similar results as the experimental results. However, in terms of cracking behaviour the computational model yields slightly different results than the experiments. The shape of the cracks and the amount of cracks in the computational model differs from the experimental results. Nevertheless, it is expected that the implementation of bond-slip behaviour and a rotating crack model for the glass will improve the cracking response of the computational model. Both aspects are currently not available in the SLA approach, but will be developed in the near future.

Additionally, it is concluded that increasing the number of reduction steps for the glass in the computational model from 5 to 10, does not alter the load-displacement curve or cracking behaviour resulting from the analysis. However, increasing the number of reduction steps for the reinforcement from 5 to 10 does improve the course of the load-displacement curve. Care should be taken to accurately define the material behaviour of the steel reinforcement in the computational model to simulate yielding of the reinforcement and to allow ductile response of the beam at the post-breakage stage.

Furthermore, it is concluded that varying the shear retention factor and mesh size within the computational model changes the load-displacement curve only to a limited extend. However, varying these model factors does have a significant effect on the cracking behaviour of the model in terms of amount of cracks. For the analyses performed in this study a shear retention factor of $\beta = 0.01$ and an element size of $h = 10$ mm (beam size = 1500x120x22 mm) seems to yield computational results which are largely in line with the experimental results. Future research will investigate the effect of mesh geometry, e.g. a triangular instead of a square mesh, and mesh size in more detail.

6. References

[1] Rots, J.G. (2001), *Sequentially linear continuum model for concrete fracture*. In Fracture mechanics of concrete structures: 831-839. Rotterdam: Balkema

[2] Rots, J.G., Belletti, B. & Invernizzi, S. (2008), *Robust modeling of RC structures with an "event-by-event" strategy*. Engineering Fracture Mechanics; 75: 590-614.

[3] Rots JG, Invernizzi S. Regularized sequentially linear saw-tooth softening model. In: International Journal for Numerical and Analytical Methods in Geomechanics, Vol. 8, No. 7 – 8, pp. 821 – 856 (2004).

[4] DeJong, M.J., Hendriks, M.A.N. & Rots, J.G. (2008). Sequentially linear analysis of fracture under non-proportional loading. Engineering Fracture Mechanics 75(18): 5042-5056.

[5] Graaf, A.V. van de, Hendriks, M.A.N & Rots, J.G. (2009). *Sequentially linear analysis for modeling tunnelling-induced surface structure damage*. 2nd Int. Conf. on computational methods in tunnelling, EURO: TUN 2009 (pp. 977-984). Freiburg, Germany: Aedificatio Publishers.

[6] Graaf, A.V. van de (2008). *Sequentially linear analysis as an alternative to nonlinear analysis applied to a reinforced glass beam*. 7th fib PhD Symposium (pp. 63-71)

[7] Louter, P.C., Bos, F.P. & Veer, F.A. (2008). *Performance of SGP and adhesively bonded metal-reinforced glass beams*. ISAAG 2008 conference proceedings (pp. 203-210). Munich

[8] NEN-EN 572-1, *Glas voor gebouwen – Basisproducten van natronkalkglas – Deel 1: Definities en algemene fysische en mechanische eigenschappen*, Delft, The Netherlands, 2004

[9] Haldimann, M., Luible, A., Overend, M., Structural Use of Glass, Structural Engineering Documents 10, IABSE, Zurich, Switzerland, 2008.SED

[10] Granta Design Limited (2009), CES Edupack version 5.1.0, Material Universe Database.

[11] Trovato D. (2009) - *Sequentially linear analysis for a reinforced glass beam* (MSc. thesis), Politecnico di Torino/ Delft University of Technology